Oncogene (2004) 23, 9090–9101

www.nature.com/onc

Distinct profiles of critically short telomeres are a key determinant of different chromosome aberrations in immortalized human cells: whole-genome evidence from multiple cell lines

Wen Deng[1], Sai Wah Tsao[1], Xin-Yuan Guan[2], Joe N Lucas[3], Hua Xin Si[1], Chi Shing Leung[4], Priscilla Mak[4], Li Dong Wang[5] and Annie LM Cheung*[,1]

[1]*Department of Anatomy, Faculty of Medicine, The University of Hong Kong, 21 Sassoon Road, Pokfulam, Hong Kong, SAR, China;* [2]*Department of Clinical Oncology, The University of Hong Kong, Sassoon Road, Pokfulam, Hong Kong, SAR, China;* [3]*Lawrence Livermore National Laboratory, University of California, Livermore, CA 94550, USA;* [4]*Department of Pediatrics and Adolescent Medicine, Faculty of Medicine, The University of Hong Kong, Sassoon Road, Pokfulam, Hong Kong, SAR, China;* [5]*Laboratory for Cancer Research, Experimental Center for Medicine, Henan Medical University, Zhengzhou, Henan Province, China*

Chromosomal aberrations are common in cancers. However, the search for chromosomal aberrations leading to development of specific solid tumors has been severely hindered because the majority of solid tumors have complex chromosomal aberrations that differ within the same tumor types. A similar phenomenon exists in immortalized cell lines. The underlying mechanisms driving these diverse aberrations are largely unknown. Telomeres play crucial roles in protecting the integrity of eucaryotic chromosomes and maintaining genomic stability of human cells. Telomere lengths on individual chromosomes in normal human somatic cells are heterogeneous and undergo progressive shortening with aging process. In this study, for the first time, a molecular cytogenetic method using sequential telomere quantitative fluorescence *in situ* hybridization and spectral karyotyping on the same human metaphases was applied successfully to examine the dynamic profiles of individual telomere shortening and their relationship to chromosome aberrations in multiple human cell lines undergoing immortalization. Human ovarian surface epithelial cells and esophageal epithelial cells were immortalized by the expression of HPV16 E6 and E7, which drive cells to proliferate by inactivating p53 and Rb genes. In these cell lines, we consistently detected large-scale differences in telomere signal intensities not only among nonhomologous chromosome arms but also between some homologous chromosome arms. The cell lines derived from different donors had different profiles of critically short telomeres (lacking telomere signals). Strikingly, the different profiles of chromosomal structural aberrations in multiple immortalized cell lines were highly significantly associated with the distinct distributions of critically short telomeres in whole-genome. Since cellular immortalization is one of the hallmarks of cancer, our findings suggest that distinct profiles of critically short telomeres in different human individuals might play an essential role in determining the complex and individual-specific chromosomal structural aberrations in human solid tumors.

Oncogene (2004) **23,** 9090–9101. doi:10.1038/sj.onc.1208119
Published online 18 October 2004

Keywords: telomeres; aberrations; genome; immortalization; human

*Correspondence: ALM Cheung; E-mail: lmcheung@hkucc.hku.hk
Received 14 May 2004; revised 29 June 2004; accepted 28 July 2004; published online 18 October 2004

Introduction

Telomeres are specialized DNA–protein structures that cap and protect eucaryotic chromosomes from end-fusions and degradations, thus playing essential roles in maintaining genomic stability (Blackburn, 2001; Gisselsson *et al*., 2001, de Lange, 2002; Wright and Shay, 2002). In most normal somatic human cells, telomeres shorten with aging process (Harley *et al*., 1990; Hastie *et al*., 1990; McEachern *et al*., 2000). It is conceived that a very short telomere may fail to form the protective telomere structures (T-loop and D-loop), thus compromising chromosomal integrity (Griffith *et al*., 1999). The resulting chromosomal structural instability, characterized by continuous generation of new chromosomal structural aberrations, is an important pathway for cells to acquire multiple genetic alterations that may lead to cancer development.

Although some recurrent chromosome aberrations have been observed in given tumor types, it is well recognized that the vast majority of solid tumors have different chromosome aberrations within the same type of tumors. For example, several widely used cervical cancer cell lines (Harris *et al*., 2003), as well as prostate and breast cancer cell lines (Davidson *et al*., 2000; van Bokhoven *et al*., 2003), etc., have dramatically different karyotypes. A similar phenomenon has also been observed in immortalized cells from the same cell types (e.g. Benn, 1976; Zhang *et al*., 2004). The distinct karyotypes are often used as a tool to authenticate

specific cell lines (Drexler *et al*., 1999; Masters, 2002). However, the underlying mechanisms for the karyotype differences within specific types of tumors or immortalized cell lines are still not understood.

Studies using quantitative fluorescence *in situ* hybridization with telomeric peptide nucleic acid probes (Q-FISH) have demonstrated that individual telomere lengths in normal somatic human cells are heterogeneous (Lansdorp *et al*., 1996; Martens *et al*., 1998; Londono-Vallejo *et al*., 2001; Graakjaer *et al*., 2003). An important implication of this finding is that the telomere length heterogeneity could be linked to nonrandom chromosome aberrations in immortalized or cancer cells. Since data from telomerase knockout mice (Hemann *et al*., 2001) as well as subsets of human chromosomes (Deng *et al*., 2003a; der-Sarkissian *et al*., 2004) have shown that chromosomes with the shortest telomeres are preferentially aberrant in aged or immortalized cells, we then asked whether the different chromosomal aberrations in whole-genomes of different immortalized human cell lines are determined by inherent differences in distributions of the shortest telomeres.

To study this issue, we used multiple human epithelial cell lines expressing human papillomavirus (HPV) 16 E6 and E7 oncogenes as our experimental models. One of the major functions of the viral oncogenes is that they inactivate both p53 and RB pathways of cell cycle regulation and allow cells to continue proliferation regardless of DNA damage signals (Munger and Howley, 2002). This simulates the frequently observed phenomenon of p53 and/or RB pathway inactivation in cancer cells (Hanahan and Weinberg, 2000; Sherr and McCormick, 2002). A unique advantage of using immortalized cells is that cells at different stages of transformation, starting from early process, can be collected for dynamic comparative studies.

Results

Development of sequential telomere Q-FISH + SKY technique on the same human metaphases

Since spectral karyotyping (SKY, Applied Spectral Imaging) is a powerful tool for identification of individual chromosomes and analysis of complex aberrations in whole-genome, we sought to apply SKY and telomere Q-FISH on the same human metaphases to study the role of critically short telomeres in affecting whole-genome karyotypic outcomes in immortalized human cell lines. To the best of our knowledge, such applications in human cells have never been reported. SKY or another equivalent technique 'M-FISH' (multiplex fluorescence *in situ* hybridization, Leica Microsystems) and telomere peptide nucleic acid FISH were previously used on human cells, but not on the same metaphases (Kawai *et al*., 2002; Smogorzewska *et al*., 2002) and no quantitative telomere signal measurements on individual chromosomes were carried out in either study. SKY and telomere Q-FISH have been applied on the same mouse metaphases (Hemann *et al*., 2001). However, telomere length heterogeneity in mice is remarkably larger than that in humans and the average telomere lengths in mice are usually an order of magnitude longer than human counterparts (Zijlmans *et al*., 1997), making telomere length quantitation in mice much easier than that in humans. In the present study, we developed new FISH protocols that allowed sequential telomere Q-FISH and SKY on the same human metaphase cells. With this technique, each individual chromosome in the whole-human-genome could be identified accurately and efficiently for detailed chromosome aberration analysis and telomere signal measurements (Figure 1a and b).

Initiation of chromosomal structural instability

We started with cells from a previously established human ovarian surface epithelial cell line, HOSE 11-12, expressing HPV 16 E6E7 (donor age 49 years, Tsao *et al*., 2001), at the earliest population doubling (PD) available (PD 7). Metaphases with chromosomal ends not involved in fusions were identified for telomere signal measurements. Our data showed that telomere fluorescence intensities (TFIs) on sister chromatids were similar as observed by Lansdorp *et al*. (1996) and therefore averaged on each arm. However, we observed consistently striking differences in TFIs among nonhomologous chromosome arms as well as between some homologous chromosome arms (an example is given in Figure 1a and b). The telomere length heterogeneity was also evident in the TFI frequency distribution measured in 20 metaphases (Figure 1c). To avoid obscuring critically short telomeres, we used the counts of telomere signal-free ends on homologous chromosome arms in 20 metaphases to describe the profile of critically short telomeres. At PD 7, chromosome arms 5p, 8q, 11q, 13p, 19p, 20q and 22p had the highest frequencies of telomere signal-free ends (Figure 2a).

To further distinguish homologous chromosomes, pericentromeric band (C-band) polymorphisms were used. Among the seven pairs of chromosomes mentioned above, we found that the homologues of chromosome 5 could be distinguished from each other by their consistent differences in C-band staining. As shown in Figure 1d, one homolog (designated homolog A) had a strong DAPI staining on the pericentromeric q-arm, whereas the other (homolog B) had a light centromeric staining. Our Q-FISH analysis showed that 5p arm lacking telomere signals was always on homolog A, whereas the 5p and 5q arms of homolog B had intermediate to strong levels of telomere signals (Figure 1b and Table 1). Analysis of chromosome aberrations showed that 95% of chromosomal end-to-end fusions involving chromosome 5 occurred on the p-arm of homolog A (Table 1). Examples are given in Figure 3a–f, which show end-to-end fusions between 5p of homolog A and 19p, as well as between 5p of homolog A and 20q in two different metaphases. It is to be noted that the fusion sites did not have detectable telomere signals, and that 19p and 20q were also among

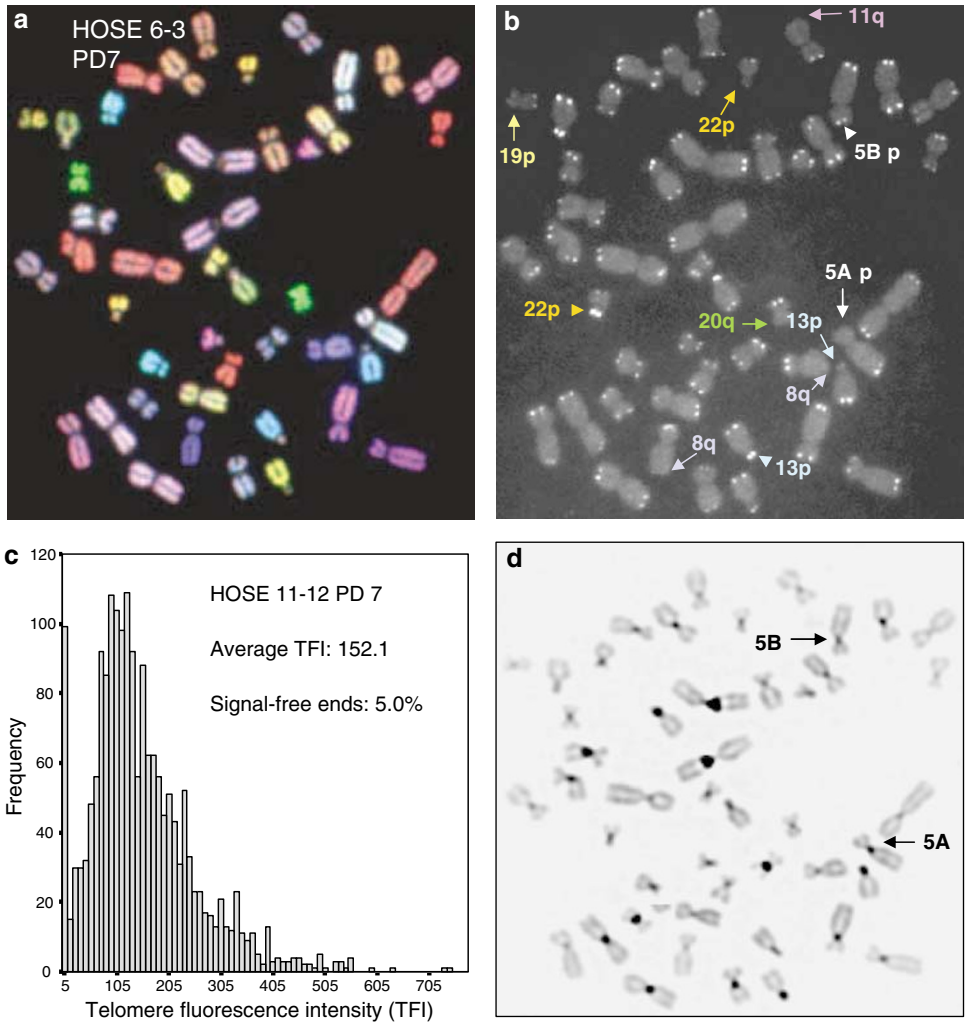

Figure 1 SKY, telomere signals and C-bands in a HOSE 11-12 cell at PD7. (**a**) SKY-stained chromosomes. (**b**) Telomere signals on individual chromosomes in the same metaphase as (**a**) Black-and-white telomere images were taken for telomere signal quantification. Arrows indicate chromosomal ends with shortest telomeres. Arrowheads indicate chromosomal ends showing striking differences in telomere signal intensities compared with those on their homologous chromosomal ends. (**c**) TFI frequency distribution measured in 20 metaphases. (**d**) C-bands in the same metaphase as (**a**) Note the dark stain at the pericentromeric region of a 5q arm (homolog A) and light stain at the pericentromeric region of homolog B

the chromosome arms with the highest frequencies of telomere signal-free ends in this cell line.

However, most homologues were not always distinguishable from each other based on C-band variations. We also used chromosome arm-specific subtelomeric probes (from Vysis) seeking to distinguish between homologous chromosomes, but unfortunately, found no consistent variations in subtelomeric signals on this set of chromosomes with critically short telomeres in this cell line. We therefore pooled the data for the same arms of both homologues for consistency in presenting whole-genome data. In general, our results showed that the frequencies of chromosomal structural aberrations were not randomly distributed. These aberrations at PD 7 occurred preferentially on the chromosome arms that had the highest frequencies of telomere signal-free ends (Figure 2b). Most ($\sim$3/4) of the structural aberrations at this early PD were end-to-end fusions. Other aberrations included translocations, dicentrics (not end-to-end fusions), insertions, deletions and duplications. Further analysis showed that 71% of all rearrangements (dicentrics, translocations and insertions) at PD 7 occurred on the chromosome arms with critically short telomeres mentioned above, and 22% of all aberrations involved at least one of these seven chromosomes exchanging with other chromosomes that were not identified as carrying critically short telomeres. Since chromosomal rearrangements result from DNA misrepair, our data indicate that chromosomal ends with critically short telomeres are not only prone to recombining with each other but also occasionally invade other chromosomes during DNA misrepair. It is noteworthy that no identical aberrations were observed in any of the metaphases at PD 7. This ruled out clonal

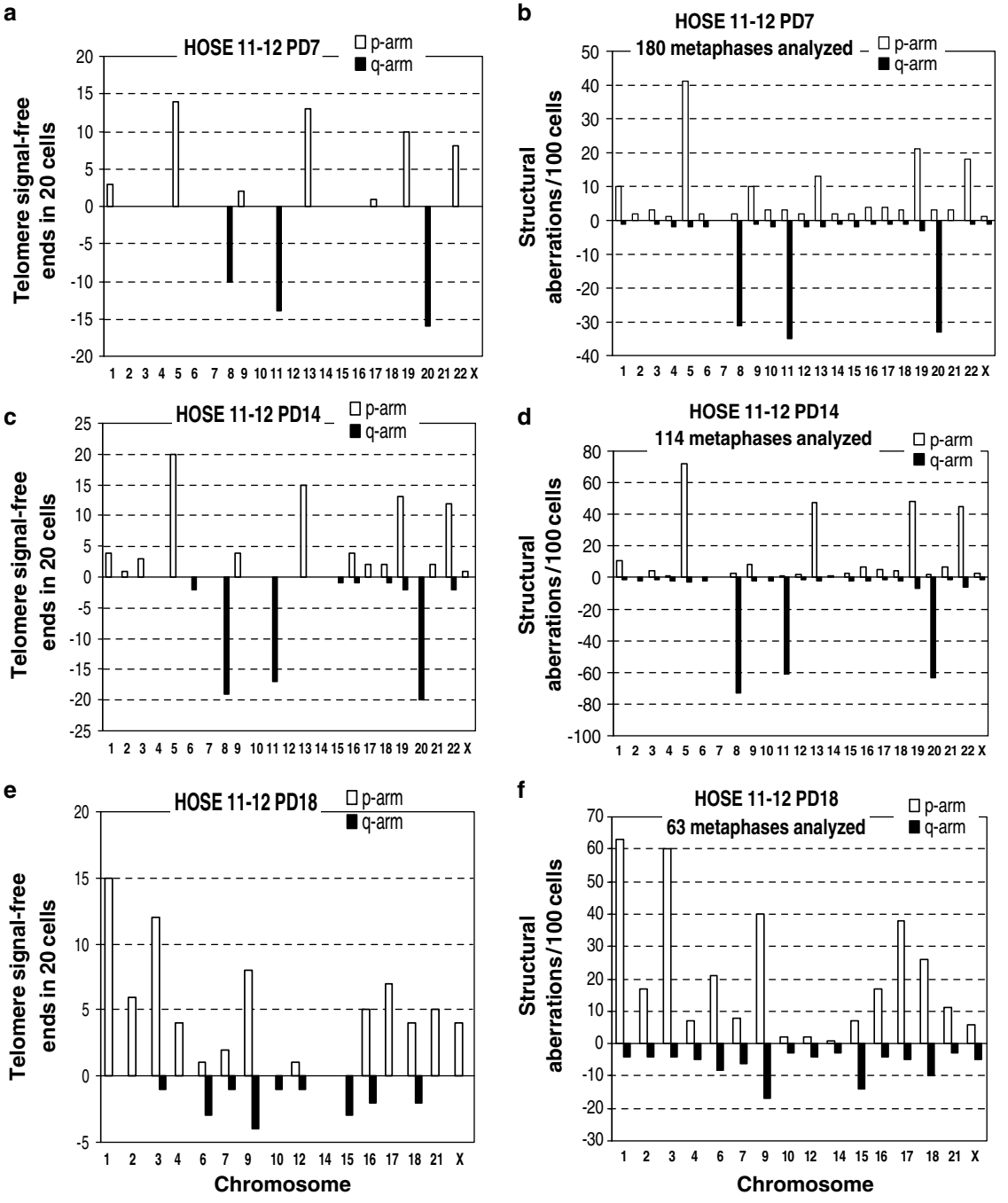

Figure 2 Frequencies of telomere signal-free ends and chromosomal structural aberrations on individual chromosomes in HOSE 11-12 cells at PD 7, PD 14 and PD 18, respectively. The correlation coefficients between the two parameters at PD 7, PD 14 and PD 18 were 0.95 ($P \leqslant 0.0001$), 0.98 ($P \leqslant 0.0001$) and 0.95 ($P \leqslant 0.0001$), respectively. Note that by PD 18, complete telomere Q-FISH data for chromosome arms 5p, 8q, 11q, 13p, 19p, 20q and 22p were no longer available (therefore not shown in **e** and **f**) because each of these chromosome arms had at least one structural aberration in almost every metaphase analysed

expansion, but rather suggested that those aberrations with elevated frequencies were produced *de novo*.

Progression of chromosomal structural instability

To follow the evolution of chromosome aberrations in detail, we studied HOSE 11-12 cells at PD 14 (an intermediate stage towards crisis) and at PD 18 (at crisis). We observed that the seven chromosome arms that originally had the shortest telomeres persisted to have the highest frequencies of chromosomal aberrations at PD 14, and their aberration frequencies increased with population doubling coupled by increases in telomere signal-free ends (Figure 2c and d).

When HOSE 11-12 cells were at crisis (at PD 18), which was characterized by massive cell death and

Table 1 Telomere fluorescence intensity and chromosome structural aberrations on homologous chromosome 5 in HOSE 11-12 and homologous chromosome 9 in HOSE 6-3 cells[a]

Chromosome arm	*Early PD*[b]		*PD 14*		*PD 18 (crisis)*	
	TFI	*Aberrations*	*TFI*	*Aberrations*	*TFI*	*Aberrations*
HOSE 11-12						
5Ap	8.3±13.7	41	0	71	/	123
5Aq	124.6±36.2	0	68.7±25.1	2	40.2±23.7	5
5Bp	99.5±26.1	1	60.2±23.8	2	38.4±19.5	4
5Bq	223.5±58.8	1	154.1±38.9	1	121.9±35.1	3
HOSE 6-3						
9Ap	25.6±23.0	21	10.0±18.1	69	/	107
9Aq	84.9±33.9	1	51.9±35.2	2	34.6±18.3	6
9Bp	223.5±54.9	1	166.9±52.2	1	132.7±40.2	2
9Bq	308.9±83.3	0	247.8±55.9	0	201.0±51.8	1

[a]Homologues were distinguished from each other by C-band polymorphisms as shown in Figures 3 and 6. Telomere fluorescence intensities (TFI) on intact ends were measured in 20 metaphases. Aberrations per 100 metaphases were given. [b]HOSE 11-12 at PD 7; HOSE 6-3 at PD 8

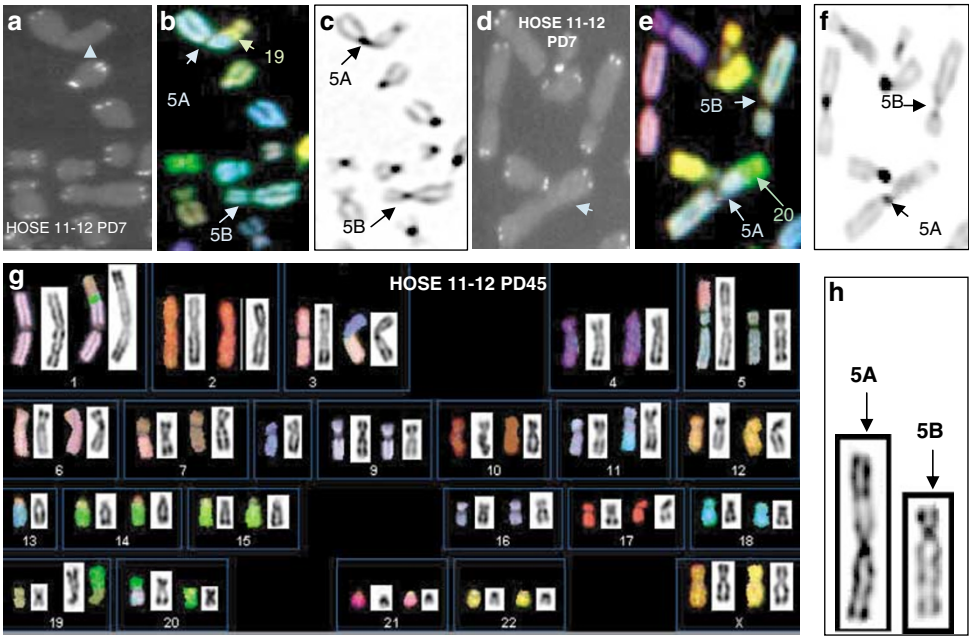

Figure 3 Typical chromosomal fusions involving chromosome 5 in HOSE 11-12 cells at PD 7. (**a**) and (**d**) show telomere signals, (**b**) and (**e**) SKY images, (**c**) and (**f**) C-bands in two metaphases, respectively. Homolog A was identified by having darker C-band stain than homolog B. Homolog 5B was intact with detectable telomere signals on both p- and q-arms, but 5p of homolog A fused with 19p as shown in (**b**) and with 20q in (**e**). Note that the fusion sites indicated by arrowheads did not have telomere signals. (**g**) SKY karyotype of a major clone in postcrisis cells at PD 45. The karyotype description is given in Table 2 (HOSE 11-12, the first clone). (**h**) C-band variations on chromosome 5 to distinguish between the homologues in the same cells shown in (**g**). The derivative chromosome 5 was homolog A, while homolog B was normal

blast-like cell morphology, these seven chromosome arms had structural aberrations in nearly every metaphase analysed so that complete telomere Q-FISH data could no longer be obtained for these chromosomes (data not shown in Figure 2e and f). In fact, most fusion sites involving the seven chromosome arms lacked telomere signals. It is noteworthy that the total frequency of translocations, insertions, deletions and duplications became higher than that of dicentrics on the seven chromosomes (relative ratio was about 3/2), displaying the evolutional late stages of their structural instability.

By analysing C-band variations on chromosome 5, we observed that 91% of structural aberrations on chromosome 5 were again on the p-arm of homolog A, whereas 5B homolog mostly remained intact with their detectable telomeres even when cells were at crisis (Table 1).

In addition to the original chromosomal ends with the shortest telomere, other chromosome arms, for example, chromosomes 1p, 3p and 9q, emerged to show elevated frequencies of telomeric fusions at PD 18 (Figure 2e and f), indicating the onset of their structural instability. This was accompanied by an increase in frequency of telomere signal-free ends on these additional chromosome arms (compared with the data in Figure 2a and c). Again, none of the analysed metaphases at both PD 14 and PD 18 had completely identical aberrations.

Table 2 Karyotypes in postcrisis cells from four human cell lines[a]

Cell line	*Karyotype of the stablized major clones in postcrisis cells*
HOSE 11-12	At PD 22 and PD 45: 44,XX,der(1)t(**1**;20)(**p**34;?)t(7;20)(q21;?),der(**3**;8)(q10;q10), der(5)t(**1**;**3**)(**p**34;q21)t(**1**;5)(**p**36;p15),der(7)t(**3**;7)(**p**21;q11), der(11)t(11;13)(q12;q12),-13,der(19)t(19;20)(p13;q?), der(20)t(**1**;11)(**p**34;?)t(**1**;20)(**p**35;q12)[26]/46,XX,der(1)t(**1**;6)(**p**13;p22), der(5)t(**1**;**3**)(**p**34;q21)t(**1**;5)(**p**36;p15),der(11)t(11;13)(q13;q12), der(19)t(**1**;6)t(**p**3?;q23)t(**1**;20)(**p**3?;?)t(19;20)(p13;?),r(19)(?), der(20)t(**1**;11)(**p**34;?)t(**1**;20)(**p**35;q12)[18]
HOSE 6-3	At PD 24 and PD 45: 43,XX,der(4)t(**1**;4)(**p**35;q11),+5,-8,der(9)t(8;9)(q11;p11), der(10)t(**10**;11)(**q**11;p11),-13,der(14)t(9;14;)(q11;p11),-16,r(20)(?), -22[25]/ 36,X,-X,del(3)(q1),der(6)t(6;14)(p23;q22),-7,der(8)t(8;18)(p11;p11), -9,der(10)t(**10**;14)(p11;q11),-13,-15,-16,-18,der(20)t(9;20)(?;p11),- 21,-22[18]
NE1-E6E7	At PD 40: 47,XY,+20,r(22)(p13q11)[21]/47,XY,der(8)t(8;13)(p21,q?),+20, r(22)(p13q11)[15]/46,XY,del(**4**)(**p**11),der(11)t(**11**;19)(**q**25;p11),- 19,+20, r(22)(p13q11)[14]
NE6-E6E7	At PD 25 and PD64: 90,XXYY,-3,-3,der(9)t(**9**;21)(**p**11;q11),del(**10**)(**q**21)×2,-12, der(14;15)(q10;q10),-17,-19,+20,+20,+20+20,+20,-21[31]

[a]The chromosome arms lacking a telomere signal in ⩾50% of measured metaphases 10 PD before crisis and during crisis are underlined and in bold type, respectively. No clonal aberrations were observed before immortalization

Collectively, these results demonstrate the fundamental role of critically short telomeres on specific chromosome arms to initiate and progressively form nonrandom chromosome aberrations before cellular immortalization.

Stabilized karyotypes in immortalized cells

Since cells acquire characteristics of immortality after surviving crisis (Wright and Shay, 1992) and immortalization is one of the hallmarks of cancer, we then studied postcrisis HOSE 11-12 cells at PD 22 and PD 45 to examine the impact of initial telomere length heterogeneity on preferential involvement of chromosomes in structural aberrations in immortalized cells. Our SKY results showed that, in contrast to precrisis or crisis cells, completely identical aberrations, but without dicentrics, existed in most metaphases at PD 22. The karyotype of a major clone in postcrisis HOSE 11-12 cells is shown in Figure 3g. It is clear that the structural aberrations were dominant derivative chromosomes with losses or gains of chromosomal elements. The summarized karyotypes are given in Table 2. The majority of clonal structural aberrations in immortalized HOSE 11-12 cells involved chromosome arms with high frequencies (⩾50%) of telomere signal-free ends before and during crisis, such as 1p, 3p, 5p, 8q, 11q, 19p and 20q. Chromosome 13 p-arm telomere dysfunction resulted in a q-arm rearrangement. Notably, C-band staining of chromosome 5 revealed that homolog A, which had critically short telomeres on its p-arm before crisis, was the homolog with the 5p rearrangement (Figure 3h). We thus conclude that the profile of critically short telomeres of HOSE 11-12 cells before immortalization had a profound impact on the specific karyotypic outcomes in immortalized cells.

The observation of identical karyotypes at PD 22 and PD 45 indicates that chromosomes (with or without aberrations) in postcrisis cells were far more stable than those in precrisis or crisis cells. This whole-genome chromosomal stabilization was accompanied by a significant decrease in overall frequency of telomere signal-free ends from 12% during crisis to less than 2% in postcrisis cells, presumably after acquiring enough genetic or epigenetic alterations to activate telomerase, which was found to be strongly positive in our postcrisis cells but negative or weakly positive in precrisis and crisis cells (Figure 4).

Different outcomes of chromosomal structural aberrations were correlated with different profiles of critically short telomeres in independent cell lines

To further investigate if the above findings were limited to a specific cell line, we extended our study to another previously established human ovarian cell line, HOSE 6-3 (Tsao *et al*., 1995), and two newly established human esophageal cell lines, NE1-E6E7 and NE6-E6E7, which were also immortalized by HPV 16 E6E7. Each of these cell lines was derived from a different adult donor (aged 45, 72, 41 years, respectively). Our Q-FISH analysis showed that each cell line had a different set of chromosome arms with critically short telomeres at PD 8–14 before crisis (Figure 5a, c and e), indicating the existence of an unidentified complex mechanism for generating and maintaining such marked differences in humans. It is noteworthy that very early NE1 and NE6 cells *before* the virus oncogene transformation (at PD 3–4) were found to have similar telomere length heterogeneities compared with those at later PDs with virus oncogene expression, except that all telomere signals were stronger at earlier PDs. Importantly, our SKY results showed that the chromosome arms that were aberrant in each cell line were strongly correlated with those having the critically short telomeres at the same PDs during the process of continual proliferation towards crisis (Figure 5). We further confirmed that, in immortalized (postcrisis) cells from these additional cell lines, most of the aberrant chromosome arms could be traced back to those chromosome arms that had high frequencies of signal-free telomeres throughout proliferation up to crisis (Table 2). Acrocentric chromosomes

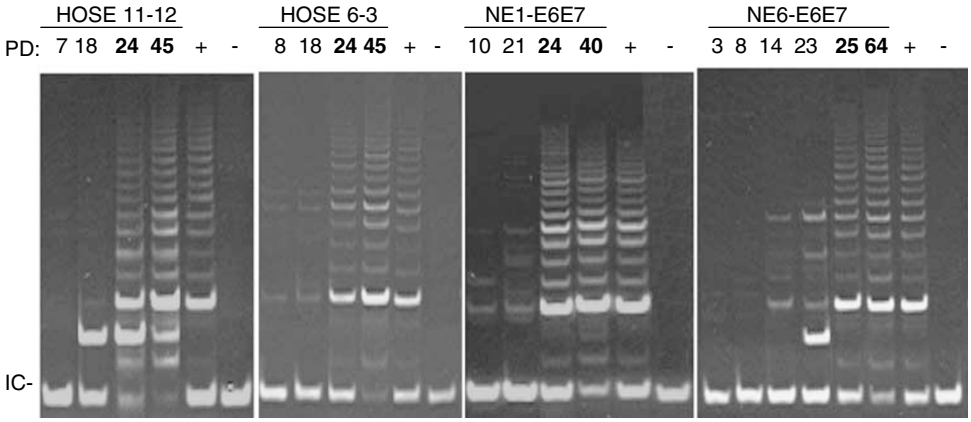

Figure 4 Telomerase activity analysed by TRAP assay. The bold PD numbers are for postcrisis cells. Protein extracted from HeLa cells and lysis buffer were included as positive (+) and negative (−) controls, respectively. A 36-bp internal standard was used as a control (IC) in the assay: the bands were weaker in samples with excessively high telomerase activity because amplification of the TRAP products and the IC bands were semicompetitive

14 in HOSE 6-3, 13 in NE1-E6E7, 14, 15 and 21 in NE6-E6E7 cells had critically short telomeres on their p-arms, which resulted in pericentromeric aberrations in immortalized cells. Again, after immortalization, the distinct karyotypes were stably propagated as evidenced by the same karyotypes observed at different postcrisis PDs. In the meantime, the total frequencies of signal-free telomeres dropped to less than 2% in each of the three cell lines, which then acquired strongly positive telomerase activities (Figure 4).

Moreover, in these additional cell lines, we found that the homologues of chromosome 9 in HOSE 6-3 cell line could be distinguished from each other by C-band polymorphism. As shown in Figure 6a–c, homolog A with smaller C-band staining had undetectable telomere signals on its p-arm and detectable telomere signals on its q-arm, whereas homolog B with larger C-band always had strong telomere signals on its p- and q-arms. About 93% of all chromosomal structural aberrations on chromosome 9 were preferentially on p-arm of homolog A, while the majority of 9B homolog was normal and had intact (although increasingly weaker) telomeres during the whole process of continued proliferation up to crisis (Table 1). Figure 6d–f show an example of chromosome fusion between terminal 9p of homolog A and intra-arm 8q, which also had critically short telomeres, and the fusion site lacked telomere signals. In postcrisis HOSE 6-3 cells, the stabilized aberration on chromosome 9 was also on the p-arm of homolog A, while the homolog B was intact as shown in Figure 6g. These results again demonstrate that only specific homologous ends with critically short telomeres were susceptible to structural instability, which then resulted in derivative chromosomes after cells become immortalized. These findings are consistent with those observed in an embryonic kidney epithelial cell line (der-Sarkissian *et al*, 2004).

It is of note that in all four cell lines, about 80% of occasional aberrations involving chromosome arms not identified as carrying critically short telomeres occurred at pericentromeric or intra-arm regions rather than at the terminal ends, and that these rearrangements involved at least one of the chromosomal arms having critically short telomeres before immortalization.

Although chromosome fusions induced by telomere dysfunction could also result in whole-chromosome losses during subsequent cell divisions, we did not detect significant correlations between profiles of critically short telomeres and chromosome numerical abnormalities beyond their ploidy in each of our cell lines. One of the reasons may be the confounding effect of HPV 16 E6E7, which also induce chromosome numerical abnormalities (Duensing *et al*., 2000). Another reason may be that the chromosomal numerical abnormalities caused by telomere dysfunction were relatively less frequent compared with structural abnormalities.

Nonlinear relationships between telomere lengths and probabilities of chromosome structural instability

In our telomere data above, the frequency of telomere signal-free ends was used as an extreme parameter for describing critically short telomeres. The dynamic data on individual arms of chromosome 5 in HOSE 11-12 cells and chromosome 9 in HOSE 6-3 cells before immortalization (Table 1) enabled us to refine the relationship between the probability of chromosomal instability and TFI on the chromosome arm of a homolog. The curve in Figure 7 plotted from the data in Table 1 clearly shows a nonlinear relationship between individual TFIs and the frequencies of *de novo* chromosomal structural aberrations. This result suggests that there is a minimum threshold of telomere length to form stable and functional telomere structures; and when its length is longer than the minimum threshold, a telomere functions normally independent of its specific length.

Of note, the whole-cell average TFIs in postcrisis cells (ranged from about 50 to 70 fluorescence values in our experiments) were even lower than those in crisis cells (ranged from about 90 to 130) despite the positive telomerase activities in postcrisis cells in our four cell

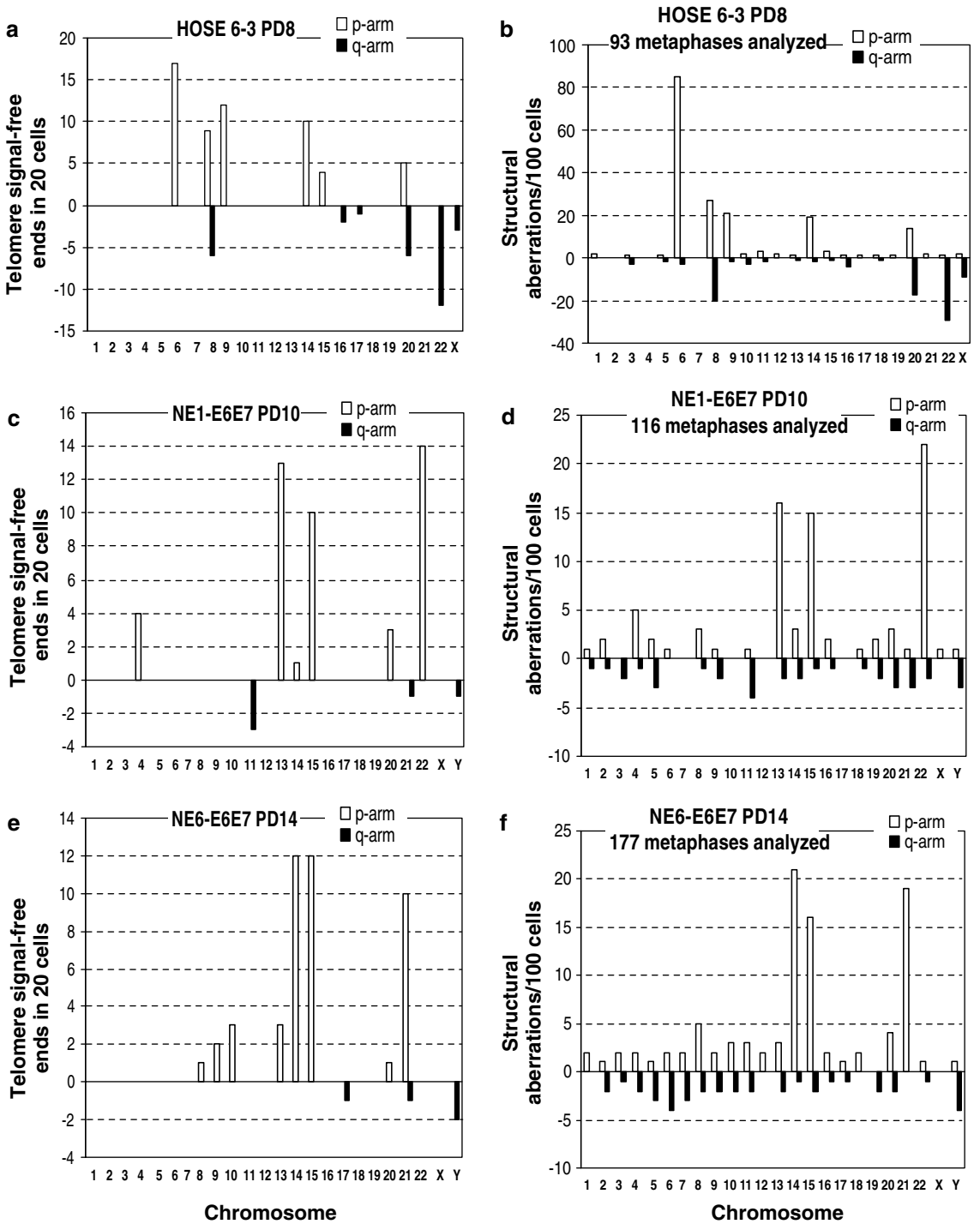

Figure 5 Frequencies of telomere signal-free ends and structural chromosomal aberrations on individual chromosomes in independent cell lines. The correlation coefficients between the two parameters in HOSE 6-3 cells at PD 8, NE1-E6E7 cells at PD 10 and NE6-E6E7 cells at PD 14 were 0.92 ($P \leqslant 0.0001$), 0.95 ($P \leqslant 0.0001$) and 0.93 ($P \leqslant 0.0001$), respectively

lines. It has been suggested that telomerase elongates telomeres most efficiently on chromosomal ends with the critically short telomeres, which leads to telomere length homogenization but not necessarily an increase in average telomere length (Ducray *et al*., 1999; Hemann *et al*., 2001). Obviously, the chromosomal stabilization in postcrisis cells cannot be explained by average telomere lengths with a linear relationship. Although we could not exclude the role of telomerase in telomere structure protection (Masutomi *et al*., 2003), our data suggest that it is also possible that the decrease in the frequencies of telomere signal-free ends rather than the overall elongation of telomeres led to the remarked alleviation of chromosomal structural instability in

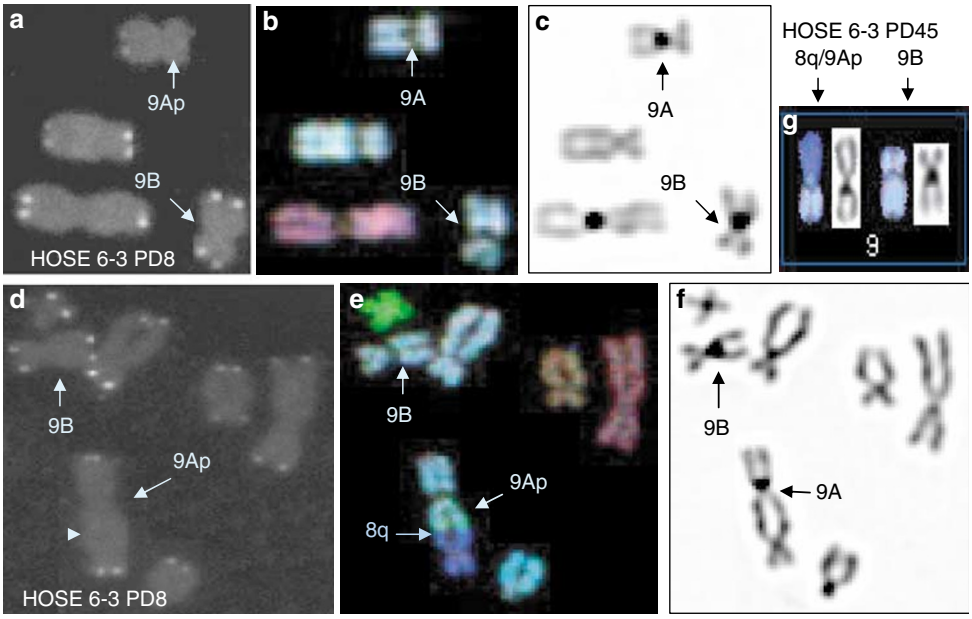

Figure 6 Typical telomere signals and a chromosomal fusion involving chromosome 9 in HOSE 6-3 cells at PD 8. (**a**) and (**d**) show telomere signals, (**b**) and (**e**) SKY images, (**c**) and (**f**) C-bands in two metaphases, respectively. Homolog A was identified by its smaller C-band than that of homolog B. The p-arm of 5A, which lacked telomere signals in the metaphase shown in (**a**), fused with 8q at an intra-arm site in another metaphase shown in (**e**). Note that the fusion site indicated by the arrowheads lacked telomere signals. The homolog 9B was intact with detectable telomere signals on both p- and q-arms. (**g**) Example of SKY and C-band variations on chromosome 9 to distinguish between the homologues in postcrisis cells. The p-arm of homolog A with smaller C-band had a translocation with 8q to produce a derivative chromosome: der(9)t(8;9)(q11;p11), whereas homolog B was normal

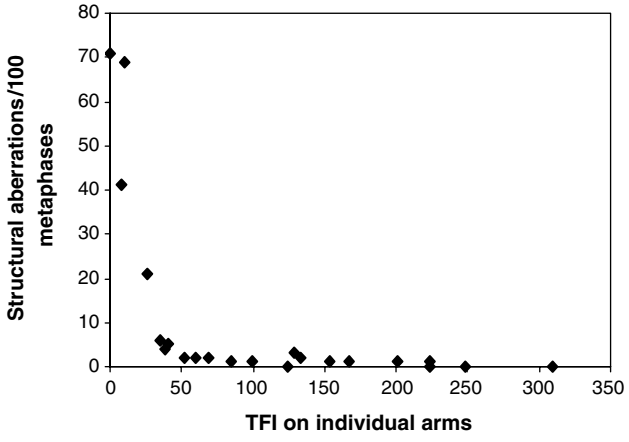

Figure 7 Relationship between frequencies of *de novo* structural aberrations and the TFIs on chromosomes 5 and 9 in HOSE 11-12 and HOSE 6-3 cells, respectively (original data from Table 1). Data from both cell lines were pooled together because they had the similar distributions

immortalized cells. These data would further support the above nonlinear model.

Discussion

It has been a long-standing mystery why specific tumors and immortalized cells have distinct karyotypes within the same tumor types or the same cell types in addition to some recurrent aberrations. In the present study, we applied telomere Q-FISH and SKY on the same human metaphases, and obtained the *whole-genome* evidence, for the first time, that diverse structural aberrations in multiple immortalized human cell lines are mainly determined by different profiles of critically short telomeres before immortalization. Our dynamic studies showed that the chromosome arms with critically short telomeres were initially predisposed to end-to-end fusions, which then resulted in derivative chromosomes after cellular immortalization, presumably after fusion-bridge-breakage cycles (de Lange, 1995) and survival selections. In particular, by distinguishing two different pairs of homologues (chromosome 5 in HOSE 11-12 cells and chromosome 9 in HOSE 6-3 cells) by C-band polymorphisms, we showed that structural aberrations starting from end-to-end fusions during the early process of immortalization to derivative chromosomes in immortalized cells were exclusively on the arm of original homolog lacking telomere signals. Derivative chromosomes in immortalized cells are often accompanied by gains or losses of chromosomal materials, as evidenced by karyotype descriptions in Table 2. These aberrations are reminiscent of the typical cytogenetic feature of human solid tumors (Mitelman *et al*., 1997; Artandi *et al*., 2000).

Several hypotheses have been proposed regarding the mechanisms for the original telomere length heterogeneity. Previous studies showed that the order of similarity between telomere length profiles in humans are: monozygotic twins > dizygotic twins > unrelated

individuals, suggesting that inherited factors may play an important role in affecting chromosome-specific telomere lengths (Graakjaer *et al*., 2003, 2004). The mechanism by which telomere length heterogeneities are generated in unrelated individuals is still unknown. It has been speculated that an individual's telomere length profile may be determined at fertilization, and the differences in telomere lengths are maintained from the zygote throughout development (Baird *et al*., 2003; Graakjaer *et al*., 2003, 2004). This is partially supported by our observation that the original shortest telomeres in cultured cells remained the shortest until fusing with other chromosomes, while the average telomere lengths became progressively shorter with more PDs. A further question is how telomere lengths are determined at fertilization. One possibility is that the telomere length profile in a fertilized cell is simply a combination of two haploid profiles, one from a germ cell in each parent, whose germ cell already has chromosome-specific telomere length heterogeneity that has accumulated gradually from previous generations. Alternatively, homologous recombination during fertilization could also produce telomere length heterogeneity. This could be supported by the facts that some human cells use homologous recombination to copy telomeric DNA from telomere to telomere as an alternative mechanism for lengthening of telomeres (ALT) (Dunham *et al*., 2000), and that intriguingly, cells with ALT usually have great heterogeneity of telomere sizes ranging from undetectable to exceptionally long within individual cells (Henson *et al*., 2002).

As to the mechanisms of telomere dysfunction, data are accumulating to show that it is ultimately the collapse of telomere loop structure that leads to the exposure of 3′ overhang and triggers DNA damage response and inappropriate DNA repair (Blackburn, 2001; de Lange, 2002; Karlseder, 2003; Li *et al*., 2003). Deficiency of telomere-associated proteins (e.g. TRF2, Ku and DNA-dependent protein kinase) compromises telomeric structure stability and leads to telomere fusions (van Steensel *et al*., 1998; Hsu *et al*., 2000; Samper *et al*., 2000; Goytisolo *et al*., 2001). In this sense, telomere shortening could contribute to the collapse of telomere loop structures in two ways. First, the double-stranded TTAGGG repeats become too short to bind enough telomere-binding proteins for T-loop formation; and second, the single stranded 3′ overhang is too short to form a displacement loop (D-loop) for the appropriate sealing of the overhang because it has been recently shown that, in addition to shortening of double-stranded telomere repeats, the 3′ overhangs also shorten with aging process (Stewart *et al*., 2003; Keys *et al*., 2004). Presently, there is no evidence to exclude either of these hypotheses. We speculate that as long as the telomeric T-loop and D-loop structures or other capping structures can be formed, a short telomere has the same protective efficiency as a longer one. This is supported by our observation that there is a clearly nonlinear relationship between telomere lengths and probabilities of chromosome structural instability.

Perhaps the most unexpected finding in this study was that, when cells were at crisis, chromosomal structural instability was not confined to those chromosomes that initially had the shortest telomeres. Progressive shortening of other original subshort telomeres further contributed to chromosomal structural instability in whole-genome, resulting in complex chromosome aberrations. We believe that this could be a general phenomenon in human cells with p53 and Rb pathway inactivation, and therefore could be relevant to cancer. This is because most human cancers have p53 and/or Rb pathway defects, which allow cells to continue proliferation regardless of DNA damage and be refractory to chromosomal structural instability on a small portion of chromosomes that originally had the shortest telomeres. The continued cellular proliferation leads to further telomere shortening on more chromosomes, so that those original subshort telomeres eventually approach dysfunctional threshold until enough genetic and or epigenetic alterations are acquired to activate telomerase for telomere elongation. We showed that, after cellular immortalization, the majority of stabilized structural aberrations could be traced back to those chromosome arms that had high frequencies of telomere signal-free ends before and during crisis. This demonstrates that the human individual-specific profiles of critically short telomeres in the whole process of immortalization (not limited to the original shortest telomeres) has a profound long-term impact on the distinct outcomes of chromosomal structural aberrations in immortalized epithelial cells derived from different donors. Since adult human tumors are predominantly of epithelial origin, the above findings may have important implications for human solid tumor development. It is tempting to speculate that distinct profiles of critically short telomeres in different human individuals may be an intrinsic genetic reason for the complex and individual-specific chromosomal structural aberrations in human solid tumors. In future studies, an additional round of FISH with probes carrying more polymorphic subtelomeric segments (such as those used by Graakjaer *et al*., 2004) before or after SKY may further enhance the ability to distinguish between homologous chromosomes in Q-FISH and aberration analysis.

Materials and methods

Cell lines and cell culture

Retroviral infection with HPV 16 E6E7 and cell culture of HOSE cells were performed as described (Tsao *et al*., 1995). Esophageal epithelial cells were grown in defined keratinocyte serum-free medium (dKSFM, Gibco, Invitrogen). Cells were fed every other day and were split 1 : 2 at early passages using trypsin–EDTA when they became near-confluent. Cells in crisis were fed three to four times weekly. Postcrisis cells were split 1 : 3 or 1 : 4 and were fed every other day.

Metaphase preparation

Metaphase cells were obtained by treatment of the cultured cells with Colcemid at a final concentration of 0.03 μg/ml for

3 h. The harvested cells were treated with 0.8% sodium citrate for 15 min at 37°C and fixed in 3 : 1 methanol/acetic acid. Cell suspension was dropped onto slides and dried as previously described (Deng *et al*., 2003b). Slides with metaphase cells were aged at room temperature (RT) for 5–7 days prior to fluorescence *in situ* hybridization.

Fluorescence in situ *hybridization*

The slides were pretreated and fixed as previously described (Deng *et al*., 2003a). The telomere probe-mix containing 7 μl hybridization buffer (Vysis Inc., Downers Grove, IL, USA) and 1 μl of 100 μM rhodamine-labeled peptide nucleic acid (PNA) telomere probe (Rho-OO-CCC-TAA-CCC-TAA-CCC-TAA) (custom PNA probe service by Applied Biosystems, Framingham, MA, USA) was denatured at 70°C for 6 min. At the same time, the slides were placed in 70% formamide/2 × SSC at 70°C for 2 min and dehydrated in ice-cooled 70, 85 and 95% ethanol for 30 s each. The slides were immediately air-dried with a nitrogen jet. The timing was controlled such that the denatured telomere probe was immediately added onto the slides right after the slides were air-dried. After hybridization at RT for 80 min, the slides were washed twice each in 70% formamide/2 × SSC at 25°C for 5 min and 2 × SSC at RT for 10 min. The slides were dehydrated in ethanol and air-dried as above. The slides were counterstained with 4′,6-diamino-2-phenylindole (DAPI) containing Antifade, covered with coverslips and viewed with a Leica fluorescence microscope. Images of telomeres were captured with CCD camera controlled by a computer using SPOT software (Leica).

Next day, coverslips were removed and the slides were washed twice in 70% formamide/2 × SSC at 37°C for 10 min and 2 × SSC at RT for 10 min, and were dehydrated in ethanol and air-dried as above. The slides were placed in 70% formamide/2 × SSC at 70°C for 4 min and dehydrated in 70, 85 and 95% ethanol for 2 min each. Other protocols including SKY probe (Applied Spectral Imaging, Migdal Ha'Emek, Israel) denaturation, hybridization and detection followed the recommendations of SKY probe manufacturer. SKY image capturing and karyotyping were performed using the SkyVision Imaging System equipped with a Zeiss Axioplan 2 fluorescence microscope. ISCN (1995) recommendations were followed in karyotype descriptions.

FISH with chromosome arm-specific subtelomeric probes and C-band staining

The slides analysed by SKY were redenatured in 70% formamide/2 × SSC at 70°C for 5 min, and were dehydrated in ethanol and air-dried as above. Probe mix consisting of 7 μl hybridization buffer and 1 μl fluorochrome-labeled chromosome arm-specific subtelomeric DNA probes (Vysis Inc., IL, USA) was denatured for 5 min at 70°C before adding onto denatured slides. After hybridization overnight at RT, the slides were washed, dehydrated and counterstained with DAPI containing Antifade and viewed with a Leica fluorescence microscope. For C-band staining, the slides after SKY or subtelomeric FISH analysis were redenatured in 70% formamide/2 × SSC at 70°C for 8 min, and were dehydrated in ethanol and air-dried. The slides were stained by DAPI and the images were captured using the SkyVision Imaging System.

Telomere signal quantitation

Individual telomere signals as telomere fluorescence intensities were determined according to the described telomere Q-FISH method (Lansdorp *et al*., 1996) using dedicated software (TFL-TELO) kindly provided by Drs Lansdorp and Poon (Poon *et al*., 1999). Telomere signals on each chromosomal end were measured in at least 20 metaphases.

Telomerase activity assay

The telomere repeat amplification protocol (TRAP) assay was performed using the TRAPEZE kit (Intergen, NY, USA) following the manufacturer's protocol. Except for negative control (lysis buffer), 0.05 μg protein was used for each PCR, which was run for 33 cycles.

Acknowledgements
We thank Drs PM Lansdorp and SSS Poon (BC Cancer Research Center, Canada) for the Q-FISH software (TFL-TELO); the Department of Pediatrics & Adolescent Medicine, University of Hong Kong, for use of SKY facilities; J Cheung, A Li, T Chan and B Lau for technical assistance. This study was supported by a grant from the Research Grants Council of Hong Kong Special Administrative Region, China (Project No. HKU 7385/03M) and a research grant from the University of Hong Kong CRCG (No. 10204355/07419/20200/323/01).

References

Artandi SE, Chang S, Lee SL, Alson S, Gottlieb GJ, Chin L and DePinho RA. (2000). *Nature*, **406,** 641–645.
Baird DM, Rowson J, Wynford-Thomas D and Kipling D. (2003). *Nat. Genet.*, **33,** 203–207.
Benn PA. (1976). *Am. J. Hum. Genet.*, **28,** 465–473.
Blackburn EH. (2001). *Cell*, **106,** 661–673.
Davidson JM, Gorringe KL, Chin SF, Orsetti B, Besret C, Courtay-Cahen C, Roberts I, Theillet C, Caldas C and Edwards PA. (2000). *Br. J. Cancer*, **83,** 1309–1317.
de Lange T. (1995). *Telomeres*. Blackburn EH, Greider CW (eds). Cold Spring Harbor Laboratory Press: NY, pp. 265–293.
de Lange T. (2002). *Oncogene*, **21,** 532–540.
Deng W, Tsao SW, Guan XY, Lucas JN and Cheung AL. (2003a). *Genes Chromosomes Cancer*, **37,** 92–97.
Deng W, Tsao SW, Lucas JN, Leung CS and Cheung AL. (2003b). *Cytometry*, **51A,** 46–51.
der-Sarkissian H, Bacchetti S, Cazes L and Londono-Vallejo JA. (2004). *Oncogene*, **23,** 1221–1228.
Drexler HG, Dirks WG and MacLeod RA. (1999). *Leukemia*, **13,** 1601–1607.
Ducray C, Pommier JP, Martins L, Boussin FD and Sabatier L. (1999). *Oncogene*, **18,** 4211–4223.
Duensing S, Lee LY, Duensing A, Basile J, Piboonniyom S, Gonzalez S, Crum CP and Munger K. (2000). *Proc. Natl. Acad. Sci. USA*, **97,** 10002–10007.
Dunham MA, Neumann AA, Fasching CL and Reddel RR. (2000). *Nat. Genet.*, **26,** 447–450.
Gisselsson D, Jonson T, Petersen A, Strombeck B, Dal Cin P, Hoglund M, Mitelman F, Mertens F and Mandahl N. (2001). *Proc. Natl. Acad. Sci. USA*, **98,** 12683–12688.
Goytisolo FA, Samper E, Edmonson S, Taccioli GE and Blasco MA. (2001). *Mol. Cell. Biol.*, **21,** 3642–3651.

Graakjaer J, Bischoff C, Korsholm L, Holstebroe S, Vach W, Bohr VA, Christensen K and Kolvraa S. (2003). *Mech. Ageing Dev.*, **124,** 629–640.
Graakjaer J, Pascoe L, Der-Sarkissian H, Thomas G, Kolvraa S, Christensen K and Londono-Vallejo JA. (2004). *Aging Cell*, **3,** 97–102.
Griffith JD, Comeau L, Rosenfield S, Stansel RM, Bianchi A, Moss H and de Lange T. (1999). *Cell*, **97,** 503–514.
Hanahan D and Weinberg RA. (2000). *Cell*, **100,** 57–70.
Harley CB, Futcher AB and Greider CW. (1990). *Nature*, **345,** 458–460.
Harris CP, Lu XY, Narayan G, Singh B, Murty VV and Rao PH. (2003). *Genes Chromosomes Cancer*, **36,** 233–241.
Hastie ND, Dempster M, Dunlop MG, Thompson AM, Green DK and Allshire RC. (1990). *Nature*, **346,** 866–868.
Hemann MT, Strong MA, Hao LY and Greider CW. (2001). *Cell*, **107,** 67–77.
Henson JD, Neumann AA, Yeager TR and Reddel RR. (2002). *Oncogene*, **21,** 598–610.
Hsu HL, Gilley D, Galande SA, Hande MP, Allen B, Kim SH, Li GC, Campisi J, Kohwi-Shigematsu T and Chen DJ. (2000). *Genes Dev.*, **14,** 2807–2812.
ISCN (1995). *An International System for Human Cytogenetic Nomenclature*. Mitelman F (ed). S Karger: Basel.
Karlseder J. (2003). *Cancer Lett.*, **194,** 189–197.
Kawai K, Viars C, Arden K, Tarin D, Urquidi V and Goodison S. (2002). *Genes Chromosomes Cancer*, **34,** 1–8.
Keys B, Serra V, Saretzki G and Von Zglinicki T. (2004). *Aging Cell*, **3,** 103–109.
Lansdorp PM, Verwoerd NP, van de Rijke FM, Dragowska V, Little MT, Dirks RW, Raap AK and Tanke HJ. (1996). *Hum. Mol. Genet.*, **5,** 685–691.
Li GZ, Eller MS, Firoozabadi R and Gilchrest BA. (2003). *Proc. Natl. Acad. Sci. USA*, **100,** 527–531.
Londono-Vallejo JA, DerSarkissian H, Cazes L and Thomas G. (2001). *Nucleic Acids Res.*, **29,** 3164–3171.
Martens UM, Zijlmans JM, Poon SS, Dragowska W, Yui J, Chavez EA, Ward RK and Lansdorp PM. (1998). *Nat. Genet.*, **18,** 76–80.
Masters J. (2002). *Int. J. Cancer*, **99,** 154.
Masutomi K, Yu EY, Khurts S, Ben-Porath I, Currier JL, Metz GB, Brooks MW, Kaneko S, Murakami S, DeCaprio JA, Weinberg RA, Stewart SA and Hahn WC. (2003). *Cell*, **114,** 241–253.
McEachern MJ, Krauskopf A and Blackburn EH. (2000). *Annu. Rev. Genet.*, **34,** 331–358.
Mitelman F, Mertens F and Johansson B. (1997). *Nat. Genet.* vol. **Spec issue,** 417–474.
Munger K and Howley PM. (2002). *Virus Res.*, **89,** 213–228.
Poon SSS, Martens UM, Ward RK and Lansdorp PM. (1999). *Cytometry*, **36,** 267–278.
Samper E, Goytisolo FA, Slijepcevic P, van Buul PP and Blasco MA. (2000). *EMBO Rep.*, **1,** 244–252.
Sherr CJ and McCormick F. (2002). *Cancer Cell*, **2,** 103–112.
Smogorzewska A, Karlseder J, Holtgreve-Grez H, Jauch A and de Lange T. (2002). *Curr. Biol.*, **12,** 1635–1644.
Stewart SA, Ben-Porath I, Carey VJ, O'Connor BF, Hahn WC and Weinberg RA. (2003). *Nat Genet.*, **33,** 492–496.
Tsao SW, Mok SC, Fey EG, Fletcher JA, Wan TS, Chew EC, Muto MG, Knapp RC and Berkowitz RS. (1995). *Exp. Cell Res.*, **218,** 499–507.
Tsao SW, Wong N, Wang X, Liu Y, Wan TS, Fung LF, Lancaster WD, Gregoire L and Wong YC. (2001). *Cancer Genet. Cytogenet.*, **130,** 141–149.
van Bokhoven A, Caires A, Maria MD, Schulte AP, Lucia MS, Nordeen SK, Miller GJ and Varella-Garcia M. (2003). *Prostate*, **57,** 226–244.
van Steensel B, Smogorzewska A and de Lange T. (1998). *Cell*, **92,** 401–413.
Wright WE and Shay JW. (1992). *Exp. Gentol.*, **27,** 383–389.
Wright WE and Shay JW. (2002). *Nat. Biotechnol.*, **20,** 682–688.
Zhang H, Tsao SW, Jin C, Strombeck B, Yuen PW, Kwong YL and Jin Y. (2004). *Cancer Genet. Cytogenet.*, **150,** 144–152.
Zijlmans JM, Martens UM, Poon SS, Raap AK, Tanke HJ, Ward RK and Lansdorp PM. (1997). *Proc. Natl. Acad. Sci. USA*, **94,** 7423–7428.